ASTFE
American Society
of Thermal and Fluids Engineers

5th Thermal and Fluids Engineering Conference (TFEC)
April 5–8, 2020
New Orleans, LA, USA

TFEC-2020-32143

CFD SIMULATION OF ISOLATED SPRAY FLASH EVAPORATION WITH ACTIVE VAPOR EXTRACTION

Guangyu Guo, Chao Zhu*, Zhiming Ji

Department of Mechanical and Industrial Engineering
New Jersey Institute of Technology, Newark, NJ 07102

ABSTRACT

Spray flash evaporation is an ultrafast evaporation phenomenon that happens when the superheated liquid is sprayed into a low-pressure environment, which has gained more attention due to the great potential in the enhancement of evaporation capacity. In the isolated evaporation of spray flash, the latent heat is self-supplied by droplets, leading to a temperature reduction in droplet residue. In an evaporator with active vapor extraction (vacuuming), there can be a significant temperature difference between the extracted vapor and discharged liquid of droplet residue. The overall evaporation capacity and the non-equilibrium in temperature between the extracted vapor and liquid residue, however, depend strongly upon the geometric design of evaporation chamber, the spray characteristics, and associated operation conditions including feeding flow rate and temperature and vacuuming pressure. Quantification of such a complicated system requires the establishment of a physical modeling and corresponding numerical simulation. This paper presents a three-dimensional CFD modeling and simulation, using ANSYS software, to investigate an isolated evaporation of spray flash in a cylindrical chamber with active vapor extraction. Due to the polydispersed atomization in spray, a two-way-coupled Lagrangian-Eulerian modeling is adopted. Discrete phase model with user-defined functions (UDF) is applied to simulate the coupled heat, mass and momentum transfer between droplets and vapor. The simulated results are compared with the experimental measurements, which shows a good agreement.

KEY WORDS: isolated evaporation of spray flash, non-equilibrium process, CFD, UDF

1. INTRODUCTION

Isolated evaporation of spray flash is an ultrafast heat/mass transfer phenomenon that happens when pre-heated droplets are suddenly sprayed into a thermally isolated and depressurized environment. With the abrupt pressure drop, the superheated droplets will evaporate immediately until reaching the saturated status of ambient pressure or being discharged out of the system. Because of the dramatic increase in evaporation area with the atomization of a liquid spray, the evaporation rate of spray flash can be much higher than that of traditional means of flash such as poor flash[1]–[3].

In an isolated evaporation of spray flash, the suddenly over-saturated droplet is forced to evaporate with the latent heat deprived of the droplet's own thermal energy. Such a process keeps going on along the path of droplet trajectory, with continued evaporation and temperature decreasing of the droplet, until the droplet reaches to thermal equilibrium with environment or exits the system. Consequently, with an active vapor extraction, such as by vacuuming, the extracted vapor has a higher temperature than that of the discharged

*Corresponding Author: chao.zhu@njit.edu

liquid residue[4]. Therefore, in an evaporator with isolated evaporation of spray flash, there exist multiple energy transfers, not only during the evaporation but also between the droplets and generated vapor.

The spray flash evaporation is a very complicated and heavily coupled process, which involves the integrated exchanges of mass, momentum, and energy between different phases and sub-volumes, as well as the phenomena of strong coupling and highly non-equilibrium on different scales [5]. Due to the introduced momentum by the spray and vacuuming, the process usually happens in a convective environment, and the relative motion between droplets and surrounding gas makes the problem even more complicated. For example: the convective boundary layer enhances the heat and mass transport on droplet's interface; the shear force on the droplet surface results in an internal circulation and increasing the internal heat transfer; the vaporization, the relative surfaces forces, and body forces will cause a varying density of gas around the droplet and complicates the flow characteristics [6].

Therefore, considering the highly-coupled heat and mass transfer with non-uniformity in spray characteristics and complex geometry of evaporator, a full scale three dimensional CFD study is necessary to evaluate the transport phenomena of spray flash. This paper presents a three-dimensional CFD simulation of isolated evaporation of spray flash in a cylindrical chamber with active vapor extraction via ANSYS. The Lagrangian -Euler method via discrete phase modeling (DPM) is adopted to investigate the transport of the spray and resulted vapor generation and extraction. Since the original DPM codes of FLUENT cannot calculate the isolated flash evaporation, the pressure-driven evaporation equation, and the coupled heat, mass and momentum transfers between droplets and continuous gas phase (vapor) have to be modified. For the convenience of comparison with available experimental results, the simulation is conducted under operation characteristics similar to that of experiment, such as atomization characteristics for initial droplet size, velocity and mass flow rates, and vacuuming pressure.

2. MODELING AND CASE SETUP

In this numerical simulation, it images the spray flash evaporation happens within an isolated evaporator that has three openings, as presented in figure 1. The vapor outlet (top) and the liquid outlet (bottom) are emphasized with the red circle. From the center hole of the top side, a continuous single-phase (water) spray with constant flow rate, size distribution, and the initial temperature is jetted into the domain. The vapor outlet is opened on the top next to the inlet; the liquid outlet is located on the pipe end of the bottom. Due to the huge volume ratio between water and vapor (around 3300:1), we assume the volumetric effect from the liquid phase will be ignored. Once the droplet hit the chamber wall, two situations will be considered: if it has already achieved the saturated status, the droplet will be assumed as immediately escaped from the chamber; if it has not become saturated yet, the droplet will continue evaporating until its temperature reach the saturation, then the left part will be treated as escaped from the chamber immediately. And in reality, the liquid outlet connects with a water reservoir, which is filled up with water that vapor cannot pass through. Therefore, the liquid outlet acts as a "wall" for the continuous phase(vapor).

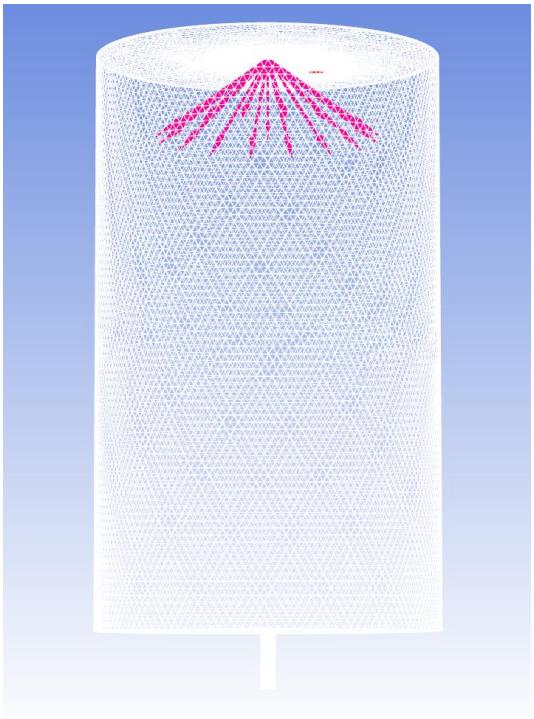

Fig 1. Geometric structure of the CFD simulation

2.1 Governing equations of continuous gas phase

In this case, the discrete phase (droplets) is strongly coupled with the continuous gas phase, and the evaporative source (vapor) constitutes the entire continuous gas phase. As each iteration of the computation, FLUENT firstly calculates the continuous phase, then performs the calculation of particle injections based on that. The results of the discrete phase will feedback and update the source terms to the gas phase for next iteration. Based on this method, we will have two coupled groups of governing equations: one set is for the continuous gas phase (vapor); the other set is for the discrete phase (droplets).

For model closure of the gas phase, the number of total independent variables should equal the number of total independent equations. As illustrated in Table 1, we have nine variables, which are density (ρ), velocity (**U**: u, v, w), pressure (p), temperature (T), Turbulent viscosity (μ_T), turbulence kinematic energy (k) and turbulence dissipation (ε). Meanwhile, we have the same amount of independent equations, which are continuity, momentum (3: u, v, w), energy, equation of state, turbulent viscosity, turbulence kinematic energy, and turbulence dissipation. The functions group is closed. Detailed major governing equations of the gas phase are summarized in Table 1.

Table 1. Major governing equations of gas phase

Continuity	$\frac{\partial \rho}{\partial t} + \nabla \cdot (\rho \mathbf{U}) = S_m$
Momentum	$\frac{\partial}{\partial t}(\rho \mathbf{U}) + \nabla \cdot (\rho \mathbf{U}\mathbf{U}) = -\nabla p + \nabla \cdot \boldsymbol{\tau} + \rho g + F_s$
Energy	$\frac{\partial}{\partial t}(\rho E) + \nabla \cdot \left[\mathbf{U}(\rho E + p)\right] = \nabla \cdot \left[k_{eff} \nabla T - (\boldsymbol{\tau} \cdot \mathbf{U})\right] + S_h$
Equation of state	$p = \rho R T$
Turbulent viscosity	$\mu_T = \rho C_\mu \frac{k^2}{\varepsilon}$

Turbulence k	$\frac{\partial}{\partial t}(\rho k)+\nabla\cdot(\rho k\mathbf{U})=\nabla\cdot\left[\left(\mu+\frac{\mu_T}{\sigma_k}\right)\nabla k\right]+G_k+G_b-\rho\varepsilon-Y_M$
Turbulence ε	$\frac{\partial}{\partial t}(\rho\varepsilon)+\nabla\cdot(\rho\varepsilon\mathbf{U})=\nabla\cdot\left[\left(\mu+\frac{\mu_T}{\sigma_\varepsilon}\right)\nabla\varepsilon\right]-\rho C_2\frac{\varepsilon^2}{k+\sqrt{\nu\varepsilon}}+C_{1\varepsilon}\frac{\varepsilon}{k}C_{3\varepsilon}G_b$

To solve this coupling problem, the source terms of the continuity equation and momentum equation are also needed to be determined. For the continuity equation, the source term S_m is use-defined and coupled with the discrete phase, which is expressed by:

$$S_m=\sum_{j=1}^{N}\sum_{i=1}^{N}\dot{m}_{vij}/V_{cell} \tag{1}$$

Where for a defined volume, i is the droplet order of one trajectory in this section, j is the local trajectory order, the sum of these two represents the total local droplet numbers. m_v is the evaporation rate of one single droplet which will be discussed in discrete phase modeling later. V_{cell} is the corresponding cell volume, and S_m is locally volumetric averaged source term.

For the momentum equation, the F_s item as a momentum source is also coupled with the discrete phase. For every single droplet based on momentum balance, the force source to the continuous gas phase can be expressed by :

$$F_{ij}=\frac{du_d}{dt}(m_d+m_a)\Delta t \tag{2}$$

Where Δt is the computational time step, the acceleration term will be discussed in discrete phase modeling later. The volumetric averaged source item for each calculational cell could be obtained as:

$$F_s=\sum_{j=1}^{N}\sum_{i=1}^{N}F_{ij}/V_{cell} \tag{3}$$

2.2 Governing equations of continuous gas phase

For model closure of the discrete phase particle (droplet), three variables of each droplet are considered as the velocity(u_p), the temperature(T_p), and the mass(m_p). Three corresponding equations are user-defined as the momentum equation eq(4), the energy equation eq(5), as well as the evaporation equation eq(6).

For a droplet settling by gravity in a depressurized vapor flow, the motion of the droplet is governed by the momentum balance of relevant forces including the added mass force, buoyancy force, and drag force, expressed by

$$(m_d+m_a)\frac{du_d}{dt}=\frac{\pi}{6}d_d^3(\rho_d-\rho_v)g-C_D\frac{\pi}{4}d_d^2\frac{\rho_v(u_d-u_v)^2}{2} \tag{4}$$

Since the droplets are under a single gas phase environment (pure vapor) with 100% relative humidity, the boiling process is assumed there is only mass transfer between droplets and continuous gas. Therefore the energy equation is expressed by

$$m_d c_d\frac{dT_d}{dt}=hA_d(T_\infty-T_d)-\frac{dm_d}{dt}h_{fg}+A_d\varepsilon_d\sigma(\theta_R^4-T_d^4) \tag{5}$$

Under the active vacuuming operation, the evaporation rate of the droplet is controlled by the pressure difference between the saturated vapor pressure at the droplet temperature and the ambient pressure controlled by vacuuming. Hence, the evaporation rate could be determined from the modified Hertz-Kundsen relation [7]:

$$\dot{m}_v=\alpha\pi {d_d}^2\sqrt{\frac{M_v}{2\pi RT_d}}\left(P_{sat}-P_0\right) \tag{6}$$

where α is the evaporation coefficient, and it needs to be experimentally determined [8]. M_v is the molecular weight of the vapor, R is the universal gas constant, P_{sat} is the saturated vapor pressure at T_d, and P_0 is ambient pressure.

2.3 Case setup

Based on the case statement, boundary definitions are summarized in Table 2. As one necessary initial condition, droplets sizes distribution and the average velocity of the spray are experimentally determined via a laser-scanning added optical measurement system [8]. The calibrated inlet spray, as well as geometric information of the evaporator, are summarized in Table 3. To validate the numerical results with the experimental results, the operating conditions as listed are keeping the same for both CFD simulation and experiments. The temperature depended polynomial relations of physical properties used in user-defined modeling are summarized as Table 4.

Table 2. Boundary conditions

Boundary	Conditions
Inlet	Mass flow inlet (zero-in); DPM inlet
Steam outlet	Pressure outlet; DPM escape
Water outlet	Mass flow outlet (zero-out); DPM escape
wall	No heat flux; DPM escape

Table 3. Spray calibration and geometric information

Parametric	Value	Unit
Spray pattern	Full-cone	N/A
Spray angle	57	degree
Spray fluid	water	N/A
Photo area (vertical direction)	139-258 (nozzle exit is 0)	mm
Photo area (horizontal direction)	0-179 (spray central axis is 0)	mm
spray diameter distribution (Rosin-Rammler)	$1-Q=\exp-(D/0.876357)^{1.4711}$	mm
Average spray velocity	3.23m/s	m/s
Mass flow rate	0.0441	Kg/s
Nozzle arrangement	one at center	N/A
Numbers of nozzle	1	N/A
Chamber height	0.5	m
Chamber diameter	0.3	m
Vapor outlet diameter	0.01905	m
Liquid outlet diameter	0.0127	m
Chamber material	Stainless steel with insulation	N/A

Table 4. Temperature dependency of phase properties

equations	remarks
$h_{fg}=aT^2+bT+c$	a=-1.794;b=-2256;c=2.5e6
$\rho_v= aT^3+bT^2+cT+d$	a=1.063e-6;b=-7.363e-5;c=0.002929;d=-0.01492
$u_v=aT+b$	a=4.031e-8;b=7.882e-6
$c_l= aT^4+bT^3+cT^2+dT^1+e$	a=1.815e-6;b=-4.754e-4;c=0.052;d=-2.139;e=4207
$c_{pv}= aT^2+bT+c$	a=0.01609;b=0.07276;c=1859

4. RESULTS AND DISCUSSION

4.1 Simulation of one typical operating condition

Grid sensitivity analysis was conducted on three different mesh density to ensure the results are in-dependent of the grid, the total cell number are 0.28million, 0.6 million and 1million, respectively. A ten seconds operating was simulated, and it was found that the converged solution does not change significantly after 0.6 million. To reduce the computational cost, the 0.6 million case is adopted.
The CFD case is simulated with the operational vacuuming pressure of 40kpa and 367K inlet temperature of the spray, and all other operating conditions are followed as Table 3. A pseudo-transient method has been used to run the simulation and until the critical variables become time non-sensitive (300 seconds in this case), such as distributions of temperatures, velocities of both two phases, as well as yield rate.

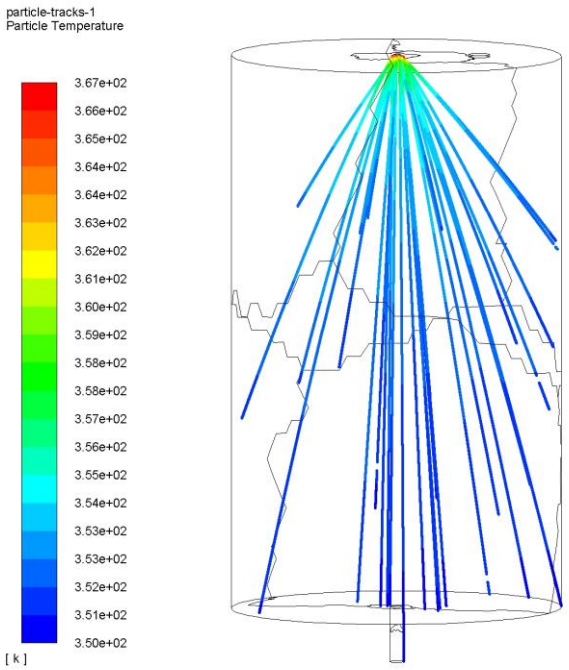

Fig 2. droplets temperature along its trajectory

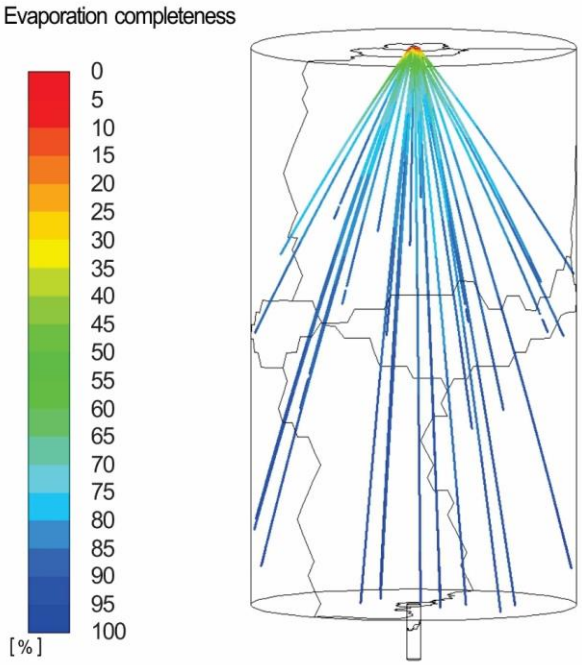

Fig 3. droplets evaporation completeness

Based on the size distribution function as mentioned above, the injection is defined as coming with ten groups of different sizes of droplets in each parcel. However, to unify the droplet size influences on the evaporation rate, one sample size of the median diameter (1.03mm) has been picked and presented in figure 2 to show the temperature changing trend. In this sample, the droplets almost achieve saturated temperature (350K) before hitting the wall. In fact, the Sauter mean diameter d_{32} in the case is about 0.3mm, which means most droplets have enough time to reach the saturated status within the travel. It also indicates the current size of the evaporator is over-designed, some optimal considerations could be done in the future.
Figure 3 shows the evaporation completeness of the sampled droplets, which is based on the mass change along the trajectory. In fact, both the mass change and temperature change are representing the evaporation process and follow the same trend as expected. In addition, both results indicate the flash evaporation is very fast that it only needs around 1/5 lengths of the entire height of the chamber to complete the most process. A cut-off reference based on the evaporative completeness could be discussed in the future to optimize the design of the evaporator.

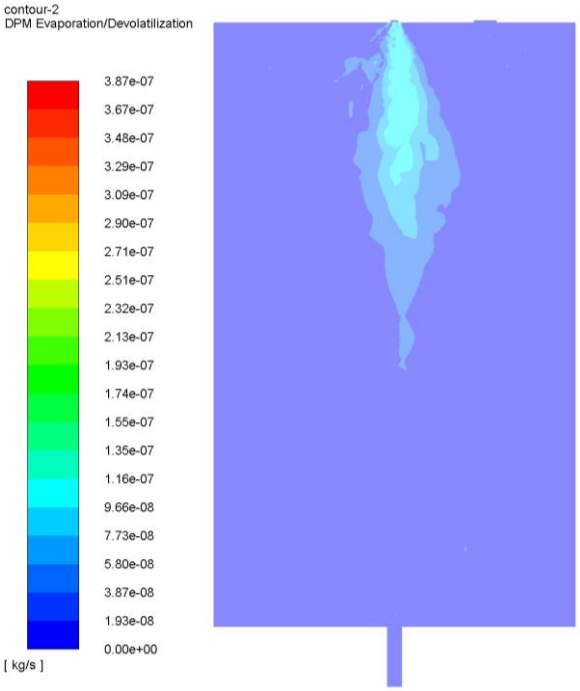

Fig 4. the contour of vapor source

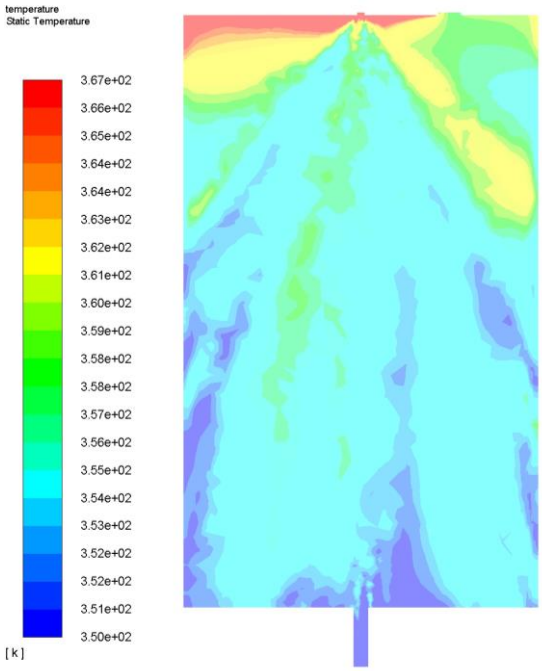

Fig 5. the contour of vapor temperature distribution

Figures 4 and 5 show the vapor source for the gas phase and temperature gradient caused by the spray evaporation. Apart from the temperature and mass change of the droplets, Figure 4 also indicates that most vaporization happens at the upper center zone of the chamber. Figure 5 shows the temperature distribution within the chamber. It clearly shows the spray evaporation introduced the hotter vapor, the hottest vapor generated and accumulated around the top zone of the chamber, and the vapor becomes cooler and cooler down the stream. Around the exit, hotter fresh vapor and cooler vapor get mixed and then finally extracted out through the steam outlet.

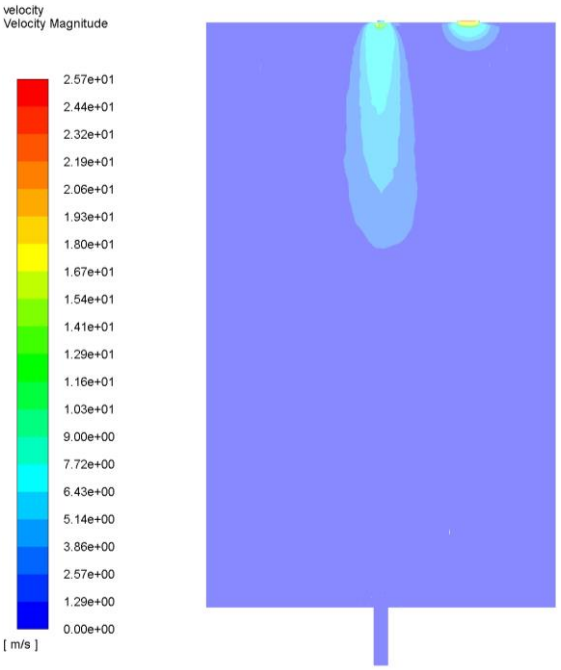

Fig 6(a). Velocity magnitude of vapor

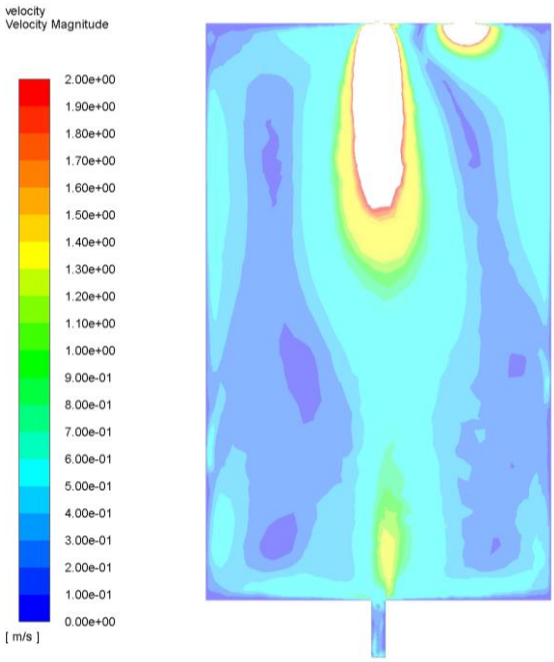

Fig 6(b). Velocity magnitude with focused range

Figures 6(a)&(b) show the velocity distribution of the vapor within the chamber. Since the overall scale cannot clearly reflect the detailed velocity distribution in most areas, where the velocity is much slower than the one of vapor outlet area, a range focused (0-2m/s) figure is also supplied.
The result indicates due to the downward movement of the droplets, the generated vapor also comes with a downward initial velocity. Some convective movements and accumulated movements are observed based on the flow path around the bottom of the chamber. It indicates the vapor will go through a mixing process before escaped out of the chamber. And how strong this mix could be will depend on the operational conditions, such as the injected velocity of the spray and the pressure level of the vacuuming. Either a higher evaporation rate or a higher spray velocity will lead to a stronger turbulent field. In other words, those two factors could influence the uniformity of the temperature distribution as well as the residue time of the vapor. This unique phenomenon worth further study in the future. In addition, for industrial applications such as spray flash distillation, the sucking flow pattern of the steam outlet could be a concern if the velocity is high enough to suck the very small droplets into the yield path. This question also needs further study in the future.

4.2 CFD validation with experimental results

The CFD simulation is validated with the experimental results of the same operating conditions based on temperature distribution of droplets along the central vertical direction, as Figure 7. The experimental data is measured by inserting a multi-sensors thermal probe into the evaporator along with the same position and direction. The related experimental study is also submitted to this conference as another article [8].

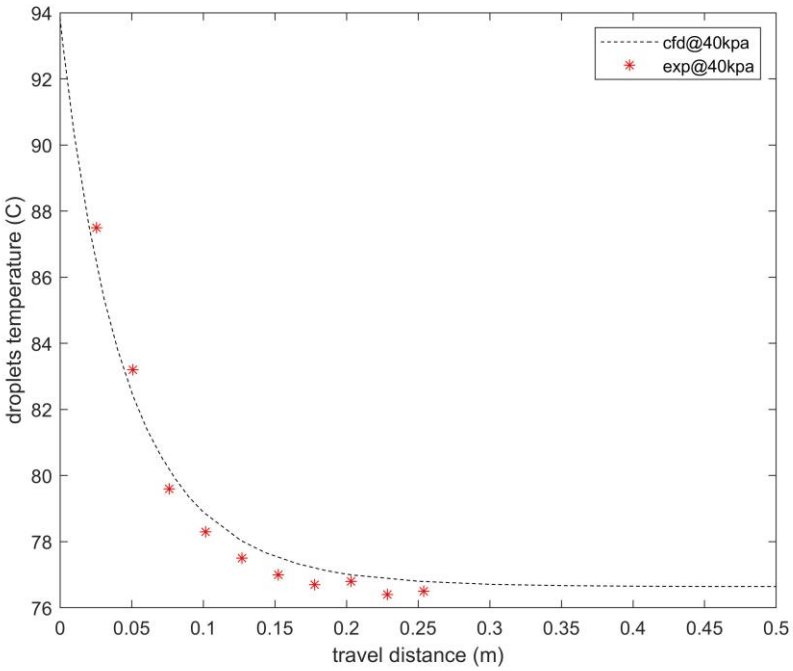

Fig 7. Comparison of droplets temperature along the vertical travel distance

Since the droplet's temperature also depends on its size, the bigger the droplet is, the smaller the temperature gradient will be. To effectively validate the result with experimental data, the droplets in CFD which are Sauter Mean Diameter and located on the vertical central path are sampled for the comparison. The red squares are the data measured from the experiments. Since the thermal probe only has 10 sensors and limited length, the last reading stops around 0.26m. However, comparing the last value of the probe and the temperature at the water outlet, a similar reading in this case indicates the thermal probe still successfully covers most part of the evaporation process. The black asterisks are the 21 data that are sampled from the target trajectory of CFD along the vertical distance with an interval of 0.025m.
The comparison indicates those results meet a good agreement, although the numerical simulation obtained a little bit higher temperature curve than experimental. In fact, measuring the real droplets' temperature under

this situation is very hard, if not impossible. Because the evaporation happens all the time, under a steady-state, the sensor-measured temperature will be lower than the exact local droplet temperature due to the phase change, and how much this error would be really depends on the residue time of the droplets during the measurement.

The overall evaporation rate, the averaged outlet temperature of vapor and water, are also compared between CFD and experiments, which are summarized as Table 5. It indicates the overall estimation of the thermal performance meets a good agreement.

Table 5. comparison of overall characteristics

	CFD	experiment
Evaporation rate	4.30 kg/h	4.19kg/h
Outlet temperature of the vapor	357.4K	357.8K
Outlet temperature of the water	349.9K	350.2K

5. CONCLUSIONS

This paper presented a three dimensional CFD study of simulating isolated evaporation of spray flash in an evaporator with active vapor extraction. Governing equations are modified for the mass and momentum transfers between vapor and droplet phases, as well as for the pressure-driven evaporation process. These modifications are implemented, via user-defined functions, into the discrete phase model in ANSYS. The simulated operation is for a cylindrical evaporator under vacuuming at 40kPa pressure and a single nozzle water spray at inlet temperature of 367K. The water spray follows the Rosin-Rammler size distribution with an averaged size of 1 mm. The simulation suggests a very fast evaporation process of spray flash so that most of droplets achieve near-equilibrium status before discharged. It clearly shows the non-uniform distribution in temperature and velocity of vapor, and the extracted vapor has a higher temperature than the liquid residue. The motion of droplets and vacuuming also affect the vapor distribution, leading to the existence of some vortices of vapor. As expected, a spray with higher injection velocity makes a deep penetration of hot vapor and hence less temperature non-uniformity due to the increased mixing effect.

NOMENCLATURE

A	projected area	(m^2)	C	drag coefficient	(-)
c	specific heat	(kJ/kgK)	d	diameter	(m)
F	force	(N)	h	heat	(J)
M	molecular weight	(kg/mol)	m	mass	(kg)
n	number	(-)	P	pressure	(Pa)
R	universal gas constant	(J/molK)	T	temperature	(C)
t	time	(s)	u	velocity	(m/s)
V	volume	(m^3)			

Greeks

α	evaporative coefficient		ε	Dissipation/emiissivity	
ρ	density	(kg/m^3)	μ	dynamic viscosity	(kg/m·s)
Δ	difference				

Subscripts

A	area	a	added mass

ch	chamber	*d*	droplet, drag
e	end	*j*	trajectory number
i	order number	*l*	water
m	modified phase	*fg*	latent heat
p	specific heat of gas phase	*sat*	saturated condition
v	vapor	*0*	ambient, initial condition

REFERENCES

[1] O. Miyatake, T. Tomimura, Y. Ide, and T. Fujii, "An experimental study of spray flash evaporation," *Desalination*, vol. 36, no. 2, pp. 113–128, Feb. 1981.

[2] O. Miyatake, T. Tomimura, Y. Ide, M. Yuda, and T. Fujii, "Effect of liquid temperature on spray flash evaporation," *Desalination*, vol. 37, no. 3, pp. 351–366, Jun. 1981.

[3] M. Maria Antony Raj, K. Kalidasa Murugavel, T. Rajaseenivasan, and K. Srithar, "A review on flash evaporation desalination," *Desalin. Water Treat.*, vol. 57, no. 29, pp. 13462–13471, Jun. 2016.

[4] G. Guo, H. Deng, C. Zhu, and Z. Ji, "Non-equilibrium evaporation in a vacuum spray flash," presetation on *4th thermal and fluids engineering conf.*, 2019.

[5] W. A. Sirignano, *Fluid Dynamics and Tandsport of Droplets and Spray*. Cambridge University Press, 2010.

[6] B. Cai *et al.*, "Mathematical study of spray fl ash evaporation in a spray-assisted seawater desalination chamber," *Desalination*, vol. 465, no. March 2018, pp. 25–37, 2019.

[7] A. H. Persad and C. A. Ward, "Expressions for the Evaporation and Condensation Coefficients in the Hertz-Knudsen Relation," *Chem. Rev.*, vol. 116, no. 14, pp. 7727–7767, Jul. 2016.

[8] G. Guo, H. Deng, C. Zhu, and Z. Ji, "Modeling and experimental study of non-equilibrium isolated spray flash evaporation," 2020, submitted to *5th thermal and fluids engineering conf.*, 2020.